

Supporting Information

**Multi-scale regulation of structure and material for  
visible-infrared- LiDAR multispectral camouflage**

*Xinpeng Jiang<sup>1,#</sup>, Jie Nong<sup>1,#</sup>, Wenhao Yuan<sup>2,#</sup>, Xin Li<sup>1</sup>, Junxiang Zeng<sup>1</sup>,  
Xinye Liao<sup>1</sup>, Qi Jiang<sup>1</sup>, Jianjing Zhao<sup>1</sup>, Zhaojian Zhang<sup>1</sup>, Sha Huang<sup>1</sup>,  
Huan Chen<sup>1</sup>, Xin He<sup>1</sup>, Jiagui Wu<sup>3</sup>, Peiguang Yan<sup>2</sup>, Junbo Yang<sup>1</sup>*

*<sup>1</sup>College of Sciences, National University of Defense Technology,  
Changsha 410073, China*

*<sup>2</sup>College of Physics and Optoelectronic Engineering, Shenzhen University,  
Shenzhen 518060, China.*

*<sup>3</sup>School of Physical Science and Technology, Southwest University,  
Chongqing 400715, China*

*<sup>#</sup>These authors contributed equally*

*\* Corresponding author: yangjunbo@nudt.edu.cn,*

*zhangzhaojian@nudt.edu.cn, chenhuan11@nudt.edu.cn (Huan*

## Supplementary Note S1. Framework of the color difference

**evaluation** The observed coloration in our device originates from the selective reflection of sunlight within the visible spectrum (0.38–0.78  $\mu\text{m}$ ). This phenomenon depends on three key elements: the properties of the illumination source, the spectrum characteristics of the device, and the perceptual response of the observer. Incident light from the illuminant interacts with the surface of the opaque structure; a portion of this light is absorbed, and the remainder is reflected. The reflected component is detected by photoreceptors to generate electrical signals that ultimately give rise to the subjective experience of color.

To quantitatively characterize this process, the International Commission on Illumination (CIE) employs a system based on three primary colors of red, green, and blue and expressed as <sup>[1,2]</sup>

$$\begin{aligned} X &= k \int_{380}^{780} R(\lambda) D_{65}(\lambda) \bar{x}(\lambda) d\lambda, \\ Y &= k \int_{380}^{780} R(\lambda) D_{65}(\lambda) \bar{y}(\lambda) d\lambda, \\ Z &= k \int_{380}^{780} R(\lambda) D_{65}(\lambda) \bar{z}(\lambda) d\lambda, \\ k &= \frac{100}{\int_{380}^{780} D_{65}(\lambda) \bar{z}(\lambda) d\lambda}. \end{aligned} \quad (1)$$

Here X, Y, Z is the tristimulus values of red, green, and blue, The term  $D_{65}(\lambda)$  denotes the spectral power distribution of the illuminant; for our study, this is standardized to D65 illumination.  $R(\lambda)$  is the reflection spectrum of the device. As shown in Supplementary Figure S1, simulated

color of samples show a good agreement with experimental one in the CIE 1931 color space.

To evaluate discrepancies between colors, various color difference frameworks have been developed, including CIE-Lab, CIE-LCH, and CMC (1:c). The CIE-Lab color space utilizes three coordinates:  $l^*$  for perceptual lightness, and  $a^*$  and  $b^*$  for chromaticity indices. These are derived from the CIE-XYZ tristimulus values through the following transformations:

$$\begin{aligned}
 l^* &= 116f(Y/Y_0) - 16, \\
 a^* &= 500[f(X/X_0) - f(Y/Y_0)], \\
 b^* &= 500[f(X/X_0) - f(Z/Z_0)], \\
 f(t) &= \begin{cases} t^{1/3}, & t > (\frac{24}{116})^3 \\ \frac{841}{108}t + \frac{16}{116}, & t \leq (\frac{24}{116})^3 \end{cases}
 \end{aligned} \tag{2}$$

where  $X_0$ ,  $Y_0$ , and  $Z_0$  are the tristimulus values for a specified reference white point (D65 illumination).

Color difference ( $\Delta E$ ) between a target color ( $l_1^*$ ,  $a_1^*$ ,  $b_1^*$ ) and a compared color ( $l_2^*$ ,  $a_2^*$ ,  $b_2^*$ ) within the CIE-Lab space is quantified as the Euclidean distance:

$$\Delta E = \sqrt{(l_1^* - l_2^*)^2 + (a_1^* - a_2^*)^2 + (b_1^* - b_2^*)^2}. \tag{3}$$

Here, target color and compared color are experimental color and simulated color in Figure 1d.

## Supplementary Figure

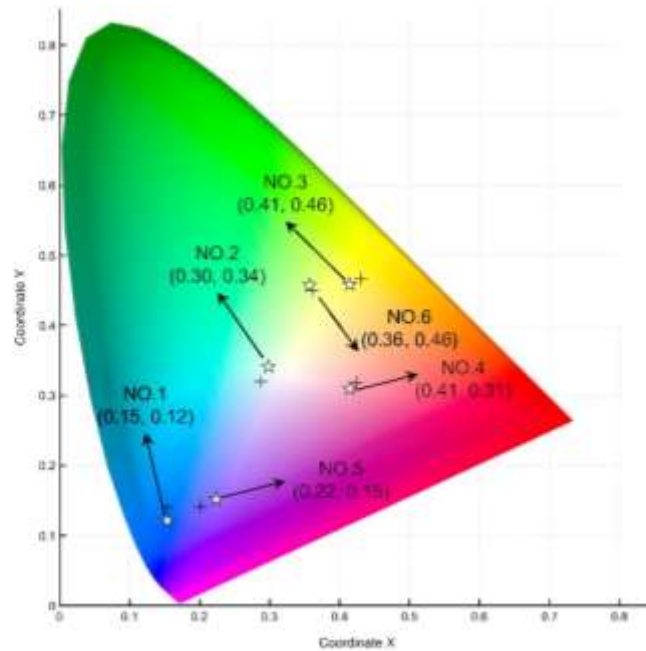


**Figure S1** Color range and distribution of the designed metadvice in CIE 1931 color space.

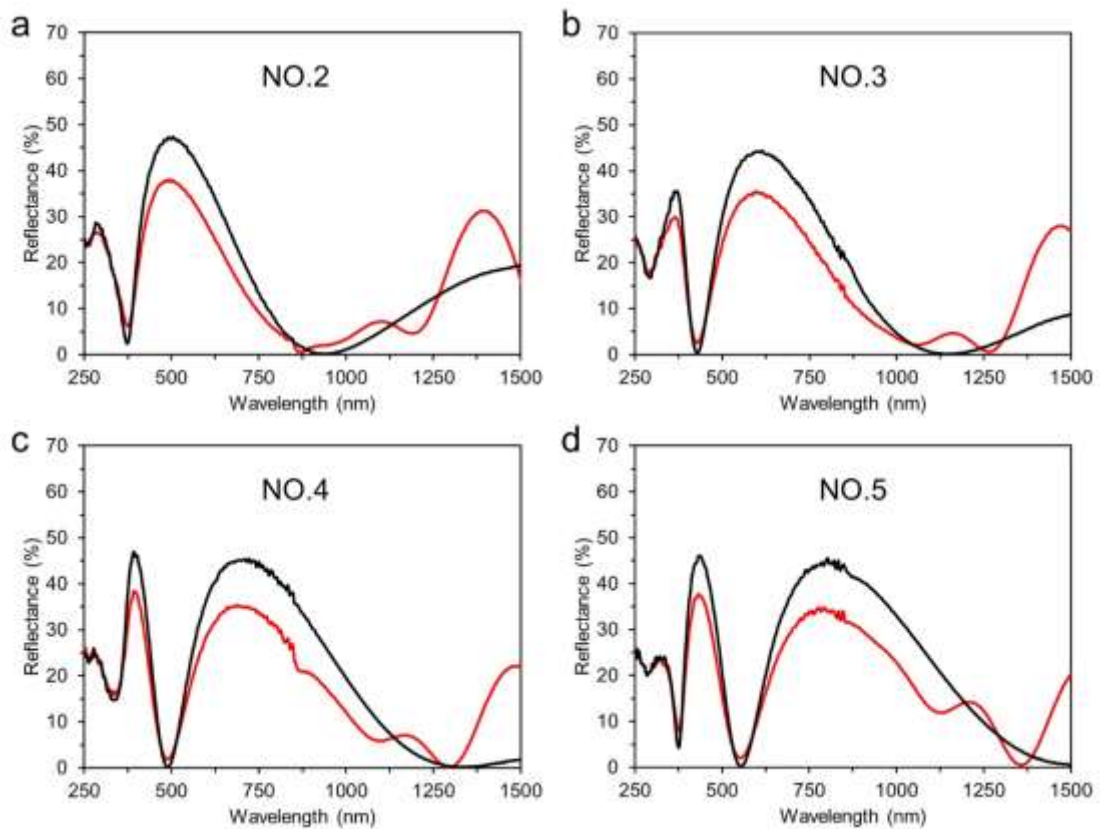


**Figure S2** The measured reflectance spectrum of samples with different thickness (a) 85 nm; (b) 120 nm; (c) 145 nm; (d) 180 nm of top ZnS layer at different state of a-GST (red line) and c-GST (black line).

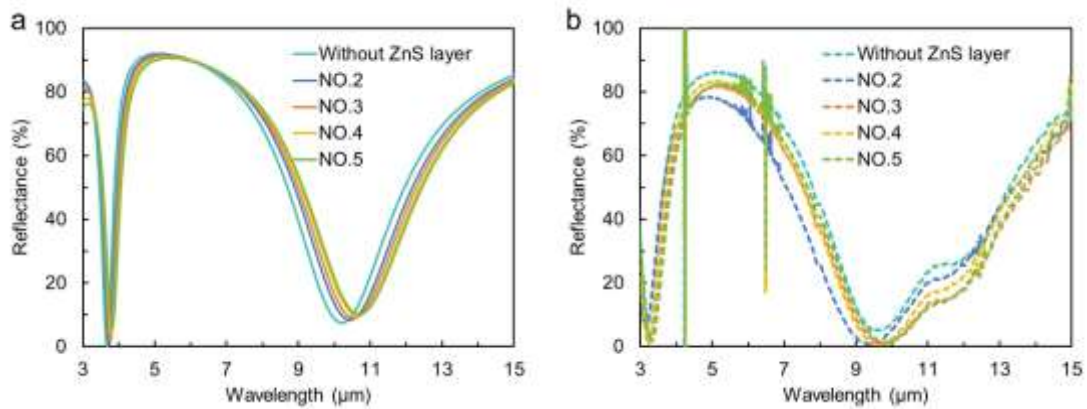


**Figure S3** The calculated (a) and measured (b) reflectance spectrum of samples with different thickness of top ZnS layer (NO.2: 85 nm; NO.3: 120 nm; NO.4: 145 nm; NO.5: 180 nm).

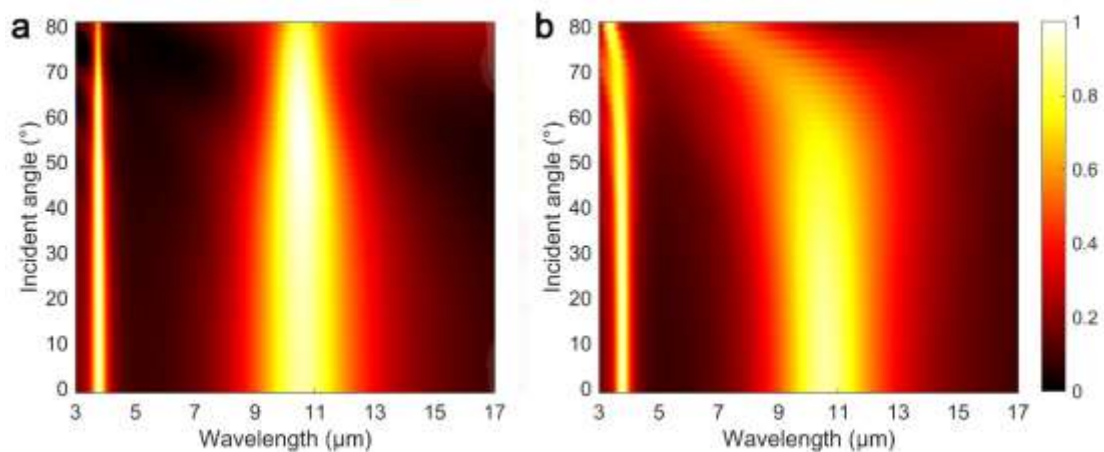


**Figure S4** Calculated absorptivity spectra of metadvice with c-GST for the P-polarization (a) and S-polarization (b) incidence.

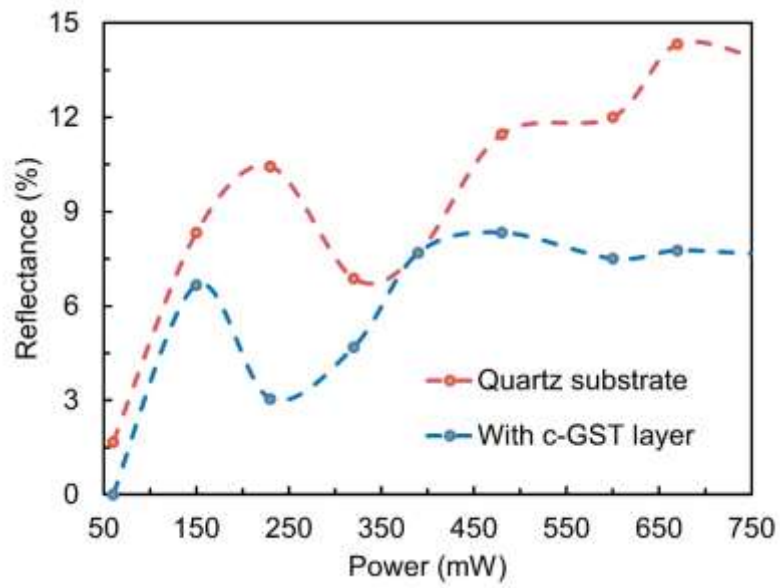


**Figure S5** LiDAR camouflage evaluation of the proposed metadvice for the wavelength of 10.6  $\mu\text{m}$  (NO.5, blue dotted line) comparing quartz (red dotted line).

## Supplementary Table

**Table S1.** Comparison of multiband camouflage devices.

Ref.	Multiband camouflage					Layer	Area
	VIS	Laser (absorption)			LMIR		
		1.06 $\mu\text{m}$	1.55 $\mu\text{m}$	10.6 $\mu\text{m}$			
3	No	98.3%	87%	83%	11%	5	100 $\times$ 100 mm
4	Yes	/	75%	80%	12%	13	200 $\times$ 200 mm
5	No	64%	90%	76%	16%	7	6-inch
6	Yes	79%	89%	80%	9%	8	6-inch
<b>This work</b>	<b>Yes</b>	<b>98.6%</b>	<b>90.1%</b>	<b>92.1%</b>	<b>42%</b>	<b>3</b>	<b>30 <math>\times</math> 30 mm</b>

**Table S2.** Comparison of wavelength-division multiplexing display devices.

Ref.	VIS	Laser	MIR
7	$\times$	$\times$	$\checkmark$
8	$\times$	$\times$	$\checkmark$
9	$\checkmark$	$\times$	$\checkmark$
10	$\times$	$\checkmark$	$\checkmark$
<b>This work</b>	$\checkmark$	$\checkmark$	$\checkmark$

## References

- [1] W. Xi, Y. J. Lee, S. Yu, et al. Ultrahigh-efficient material informatics inverse design of thermal metamaterials for visible-infrared-compatible camouflage, *Nat. Commun.* 14(1), 4694 (2023).
- [2] Y. Shi, A. Zhu, Q. Li, et al. Inverse Design of Visible-infrared Multispectral Camouflage with Radiative Cooling and Microwave Transmission, *Mater. Today Phys.* 55, 101759 (2025).
- [3] J. Huang, Y. Wang, L. Yuan, et al. Large-Area and Flexible Plasmonic Metasurface for Laser–Infrared Compatible Camouflage. *Laser & Photonics Rev.* 17, 2200616 (2023).
- [4] H. Zhu, Q. Li, C. Tao, et al. Multispectral camouflage for infrared, visible, lasers and microwave with radiative cooling, *Nat. Commun.* 12, 1805 (2021).
- [5] X. Jiang, H. Yuan, S. Ma, et al. Implementing of infrared camouflage with thermal management based on inverse design and hierarchical metamaterial. *Nanophotonics* 12, 1891-1902 (2023).
- [6] X. Jiang, J. Nong, X. Li, et al. Laser - Adaptive Inverse - Design Metamaterials for Durable Regulation from Visible - Infrared - LiDAR Compatible Camouflage to Optical Limiter. *Laser & Photonics Rev.* (2025).

- [7] R. Audhkhasi, M. R. Lien, M. L. Povinelli. Experimental Implementation of Metasurfaces for Secure Multi - Channel Image Encryption in the Infrared. *Adv. Opt. Mater.* 11(12) (2023).
- [8] X. Jiang, X. Wang, J. Nong, et al. Bicolor Regulation of an Ultrathin Absorber in the Mid-Wave Infrared and Long-Wave Infrared Regimes. *ACS Photonics* 11(1): 218-229 (2024).
- [9] Q. Chen, X. Huang, Z. Ju, et al. A Triband Metasurface Covering Visible, Midwave Infrared, and Long-Wave Infrared for Optical Security. *Nano Lett.* 25(11): 4459-66 (2025).
- [10] M. Zhang, P. Wang, X. Liu, et al. Responsive Metasurface for Directional Control of Laser and Thermal Emission Dynamic Regulation. *Adv. Mater.* 37(35) (2025).